Heat transfer during transient compression: measurements and simulations

D. R. Buttsworth
Faculty of Engineering and Surveying
University of Southern Queensland
Toowoomba, Australia 4350
buttswod@usq.edu.au

Abstract

Experiments have been performed to assess the utility of unsteady one-dimensional heat conduction modelling for the calculation of heat losses during a free piston compression process. Heat transfer measurements have been obtained within a gun tunnel barrel using surface junction thermocouple instrumentation. The gun tunnel was operated with a relatively heavy piston such that the shock waves induced by the piston motion were weak. Peak heat transfer values are estimated reasonably well by the unsteady one-dimensional model. However, overall quantitative agreement between the measurements and calculations has not been achieved at this stage, principally because the development of turbulent heat transport was not properly modelled.
keywords: heat transfer measurements, heat transfer modelling, free piston compression

1 Introduction

Transient free piston compression is a key feature of various wind tunnels, but heat transfer from the compressed gas can have a significant effect on the temperatures achieved in such facilities ([Edney, 1967]; [Knöös, 1971]; [Kendall et al., 1997]). Steady pipe flow and flat plate heat transfer correlations are popular for quasi-one-dimensional simulation of facility performance ([Groth et al., 1991]; [Jacobs, 1994]; [Tani et al., 1994]), but often these are not physically realistic models of the heat transfer during the unsteady compression processes that occur in transient wind tunnels. In contrast, unsteady one-dimensional heat transfer modelling was first applied to an IC engine many years ago (eg, [Isshiki and Nishiwaki, 1970]), and has more recently been exploited in a number of other IC engine investigations (see [Oude Nijeweme et al., 2001] and the references given therein).

Convective heat transfer can influence the operation of transient wind tunnel facilities but there is a lack of direct heat transfer measurements with supporting rational predictions in such configurations. Furthermore, unsteady one-dimensional heat transfer modelling has been quite successful in IC engine configurations. Therefore, the question addressed in this article is: can transient one-dimensional heat conduction modelling be successfully applied to the calculation of heat transfer during the compression process in a transient wind tunnel?

2 Unsteady Heat Transfer Modelling

By adopting a transformed coordinate z such that $\rho_0 dz = \rho dy$ and neglecting: (1) viscous stresses; (2) temperature gradients parallel to the surface of the wall; and (3) pressure gradients in all directions, Isshiki and Nishiwaki (1970) demonstrated that the energy equation can be written,

$$\frac{d}{dt}\left(\frac{T}{T_\infty}\right) = \alpha_0 \frac{p}{p_0}\frac{\partial^2}{\partial z^2}\left(\frac{T}{T_\infty}\right) \tag{1}$$

where the symbols have the following meanings: ρ – density; y – coordinate perpendicular to the wall; T – temperature; t – time; α – thermal diffusivity; p – pressure; and the subscripts indicate the initial (0) and instantaneous (∞) conditions outside the thermal boundary layer.

Additional assumptions made in the derivation of (1) are that the compressed air remains calorically perfect and that the thermal conductivity of the air is proportional to temperature. Both of these assumptions are reasonable in the present application due to the modest range of temperatures encountered.

Equation (1) is the well-known one dimensional heat diffusion equation with an additional time-varying coefficient, p/p_0. The boundary and initial conditions for (1) are: $(T/T_\infty)_{z=0,t} = f(t)$, $(T/T_\infty)_{z\to\infty,t} = 1$, and $(T/T_\infty)_{z,t=0} = g(z)$.

Equation (1) has been solved subject to the boundary and initial conditions using a Crank-Nicolson finite difference scheme with Gauss-Seidel iteration similar to that described by [Lawton (1987)]. The wall temperature ratio, $f(t) = T_w/T_\infty$ varies with time, principally because of the variation in T_∞. The variation in T_∞ is determined from the (measured) pressure history (Section 4.1) using the isentropic relationship.

For the present calculations, the wall temperature T_w has been assumed constant at T_w =290K. Although this is not strictly correct because of the heat transfer from the compressed gas, it is a good approximation because for the present conditions and time scales of interest, the surface temperature typically increases by around 10K, which is a small fraction of the adiabatic core temperature.

The wall heat flux is identified from the finite difference solution using the wall node and the first node from the wall in conjunction with,

$$q_w = -k_w \frac{\rho_w}{\rho_0} T_\infty \left(\frac{\partial}{\partial z}\frac{T}{T_\infty}\right)_w \tag{2}$$

where the subscript w indicates evaluation of the quantity at the wall.

The finite difference solutions of (1) used 100 nodes with grid refinement towards the wall such that the node spacing at the wall was 16 times finer than the node spacing furthermost from the wall. The node furthermost from the wall was typically located not less than 3 thermal layer thicknesses from the wall. The accuracy of the method was tested by considering the case of a material with constant thermal properties and a temperature step at the surface (there is a well-known analytical result for this case). For levels of discretization comparable to those used in the actual simulations, the finite difference results were typically within 1% of the analytical solution.

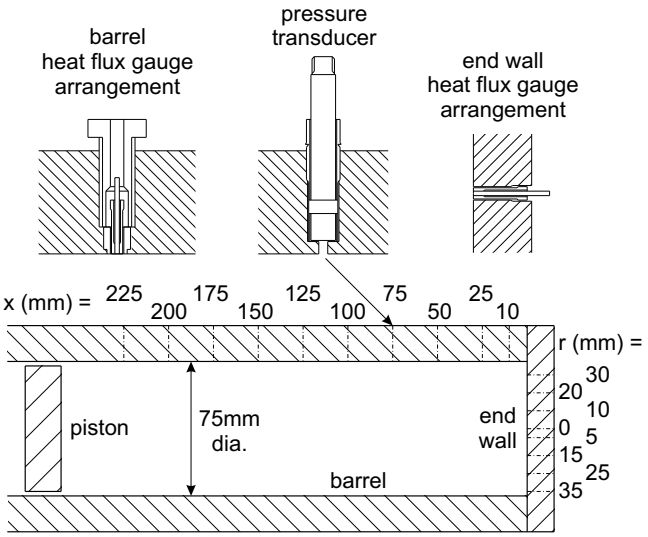

Figure 1: Schematic illustration of the barrel instrumentation.

3 Facility and Instrumentation

The transient wind tunnel used in the present work was the University of Southern Queensland Gun Tunnel. Details of the facility, its operation and performance are described elsewhere ([Buttsworth, 2002]). For the present work, the initial charge in the barrel was laboratory air at the local atmospheric pressure which was 94.1 kPa on the days of the experiments. The piston mass was 61.4 grams, and the driver was compressed nitrogen at a pressure of 3.4 MPa.

Pressure and heat flux instrumentation as illustrated in Fig. 1 was used during the experiments. Pressure was measured using a piezo-electric transducer (PCB model 112B11) in a recessed cavity at a distance of 75 mm from the end wall (see Fig. 1). At the other locations indicated in Fig. 1, surface junction thermocouples were used. The surface junction thermocouples in the barrel were glued into bushes which were themselves located on a recessed shoulder and locked in place with a nut. The barrel thermocouples were aligned with the inner surface of the barrel to within approximately 0.1 mm. The end wall thermocouples were glued directly into the end wall and were flush with the surface to within approximately 0.05 mm.

The surface junction thermocoupless are produced 'in-house' and provide a measurement of the gauge surface temperature history. The thermocouples are of an insulated coaxial construction using k-type (chromel and alumel) materials. A junction is formed close to the exposed surface of each gauge using a scratch produced by a scalpel blade. The effective thermal product of the thermocouple substrate, which is used to deduce the heat flux from the surface temperature measurements, was taken as 11400 $J/m^2 \cdot K \cdot s^{1/2}$. This value is appropriate for a scratch from the chromel to alumel substrates as used in this work. For more detail, see Buttsworth (2001).

Heat flux can be determined from measurements of surface temperature using either a digital analysis of the recorded surface temperature history, or an electrical analogue of the transient heat conduction process. Electrical analogues (along the lines described by [Oldfield et al., 1982]) were

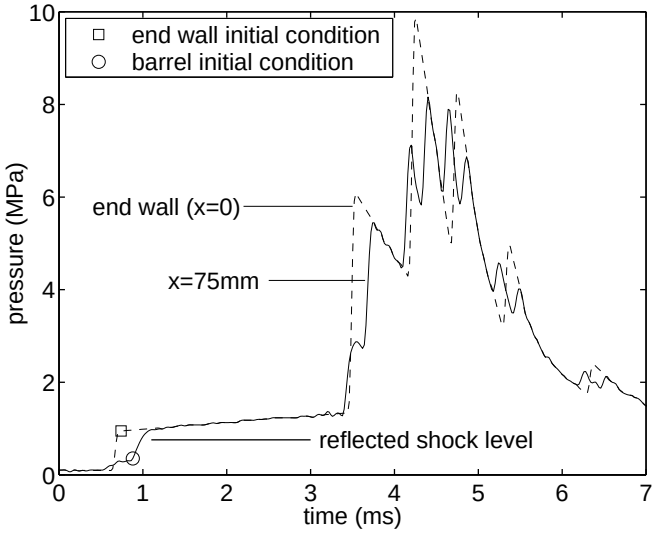

Figure 2: Pressure at the transducer station (x =75 mm) and at the end wall (x =0).

adopted for the present work because low noise heat flux data was required and the only data acquisition hardware available for the experiments reported here were 8bit oscilloscopes.

4 Results

4.1 Pressure and Temperature

Data from the pressure transducer are presented as the solid line in Fig. 2. No direct pressure measurements were made at the end wall. However, the broken line in Fig. 2 indicates the estimated pressure history at the end wall, based on linear extrapolations of the reflected shock pressures measured at x =75 mm from the end wall. To assess the validity of this extrapolation technique, a simulation of the compression process was performed using the quasi-one-dimensional routine of Jacobs (1994). It was found that extrapolation of the simulated pressure at x =75 mm from the end wall reproduced the simulated end wall pressure to within about 10%.

Incident shock arrival times were identified from the heat flux measurements on the barrel wall. The incident shock speed over the final portion of the barrel (approximately 200 mm) was 570 m/s. Such a shock produces a reflected shock pressure of about 760 kPa (as indicated in Fig. 2), whereas the measured pressure behind the reflected wave was 1.03 MPa (Fig. 2). Due to the finite length of the barrel and the relatively heavy piston used for these conditions, the isentropic compression waves associated with the initial piston acceleration process have not fully coalesced into a single compression (shock) wave by the time of arrival at the end wall.

To identify the temperature within the adiabatic core region of the compressed air, reflected shock conditions corresponding to the 570 m/s incident shock were calculated, assuming the air to be calorically perfect. Additional compression from 760 kPa up to the measured pressure of 1.03 MPa was assumed to be isentropic. Subsequent wave processes associated with the piston deceleration were

also assumed to be isentropic. This is a reasonable assumption since the majority of the entropy rise occurs with the first incident and reflected shock, and subsequent shock reflections from the piston become successively weaker.

4.2 Heat flux

Heat flux measurements and theoretical estimates at various locations are presented in Fig. 3. In the case of the end wall results (Fig. 3a), measurements from 3 locations, r =10, 15, and 20mm (see Fig. 1) are presented. Two theoretical estimates (based on the model described in Section 2), are also presented in Fig. 3a as the heavy solid lines. These calculations utilize the measured pressure history extrapolated to the end wall location as described in Section 4.1, and the corresponding adiabatic core region temperature history. The values of p_0 and T_0 used in the end wall calculations were identified from the pressure and temperature histories at the time indicated in Fig. 2 as the open square on the broken line, and a uniform initial distribution of temperature $g(z) = T_0$ was assumed.

The lower estimate in Fig. 3a is for a laminar case and uses a thermal conductivity corresponding to the laminar value for air. The upper estimate is for a turbulent case and uses a thermal conductivity value 25 times larger than the laminar value. Although this approach to modelling the turbulent transport is somewhat arbitrary, it was reasonably successful in the IC engine work of [Lawton (1987)] where peak heat flux values were correctly estimated to within about 10% (although discrepancies of 50% or more were typically apparent at other times during the IC engine cycle).

The results in Fig. 3a indicate that for the period immediately following shock reflection from the end wall, the heat flux level is slightly higher than the laminar estimate (between about 0.5 and 3.5 ms on the scale in Fig. 3a). However, with subsequent wave reflections (between about 3.5 and 6 ms on the scale in Fig. 3a), the heat flux approaches and then exceeds the turbulent estimate.

In the case of the barrel heat flux results (Fig. 3b), measurements from 2 locations, x =125 and 100 mm (see Fig. 1) are presented. Again, the solid lines represent theoretical calculations based on the model in Section 2, and the measured pressure history in Fig. 2. The values of p_0 and T_0 for the barrel predictions were identified from the pressure and temperature histories at the time indicated in Fig. 2 by the open circle on the solid line.

Since a boundary layer is established on the barrel wall prior to the arrival of the reflected shock, a nonuniform initial distribution of temperature $g(z)$ was chosen. The initial distribution was selected so that the initial heat flux was 0.5 $\mathrm{MW/m^2}$ - approximately the measured value just prior to reflected shock arrival (at around 1 ms on the scale in Fig. 3b). The choice of initial temperature distribution is not critical for the current calculations as its effects only persist for about 1 ms after shock reflection - compare the turbulent prediction in Fig. 3b (heavy solid line) with the end wall prediction (heavy broken line) in Fig. 3b.

In contrast with the end wall calculations, the laminar model does not produce a good estimate of heat flux along the barrel immediately after shock reflection (Fig. 3b between about 1 and 3.2 ms). The turbulent model appears to produce a reasonable average estimate for the reflected shock period. However, with subsequent wave reflections (between about 3.5 and 6 ms on the scale in Fig. 3b) the

turbulent model increasingly under-estimates the heat flux measurements.

The measurements and calculations of the barrel heat flux are not in-phase during the period of piston deceleration and reversal (between about 3.5 and 6 ms on the scale in Fig. 3b) because of the spatial separation of the pressure transducer (x =75 mm) and heat flux gauges. This spatial separation also leads to differences in the peak pressures at the pressure transducer and heat flux gauge stations, and contributes to differences between the measured and predicted values.

5 Conclusion

Large spatial variations in the measured heat flux have been observed. Differences in the pressure history along the barrel wall contribute to such variations, but localised differences in the turbulent transport also contribute as is evident from the measurements at the end wall.

The one-dimensional heat conduction model produces reasonable estimates of heat flux during the present transient compression process. For the calculation of turbulent heat flux, a thermal conductivity 25 times larger than the laminar value was used. The level of agreement between the model and measurements is comparable to that achieved in IC engine work - peak heat flux values are in reasonable agreement with the model, but at other times, large differences in magnitude (factors of 2 or more) are apparent.

The current model represents an improvement over quasi-steady modelling in that it provides physically sound heat flux estimates in applications where the transient response of the thermal boundary layer is important. The simplicity of the model makes it suitable for implementation in quasi-one-dimensional facility simulation routines such as those of Groth et al. (1991), Jacobs (1994), and Tani et al. (1994). However, the absolute predictive capability of the model is currently limited by the lack of a suitable model for the turbulent transport of heat. Comparison of the model results and the heat flux measurements indicates that there is an increase in the effective thermal conductivity throughout the compression process.

Acknowledgement The author wishes to acknowledge the financial support of the Australian Research Council.

References

[Buttsworth, 2002] Buttsworth DR (2002) The University of Southern Queensland Gun Tunnel: initial performance characterisation. Report TR-2002-03, Faculty of Engineering and Surveying, University of Southern Queensland, Australia.

[Buttsworth, 2001] Buttsworth DR (2001) Assessment of effective thermal product of surface junction thermocouples on millisecond and microsecond time scales. Experimental Thermal and Fluid Science 25:409–420.

[Edney, 1967] Edney BE (1967) Temperature measurements in a hypersonic gun tunnel using heat transfer methods. J Fluid Mech 27:503–512.

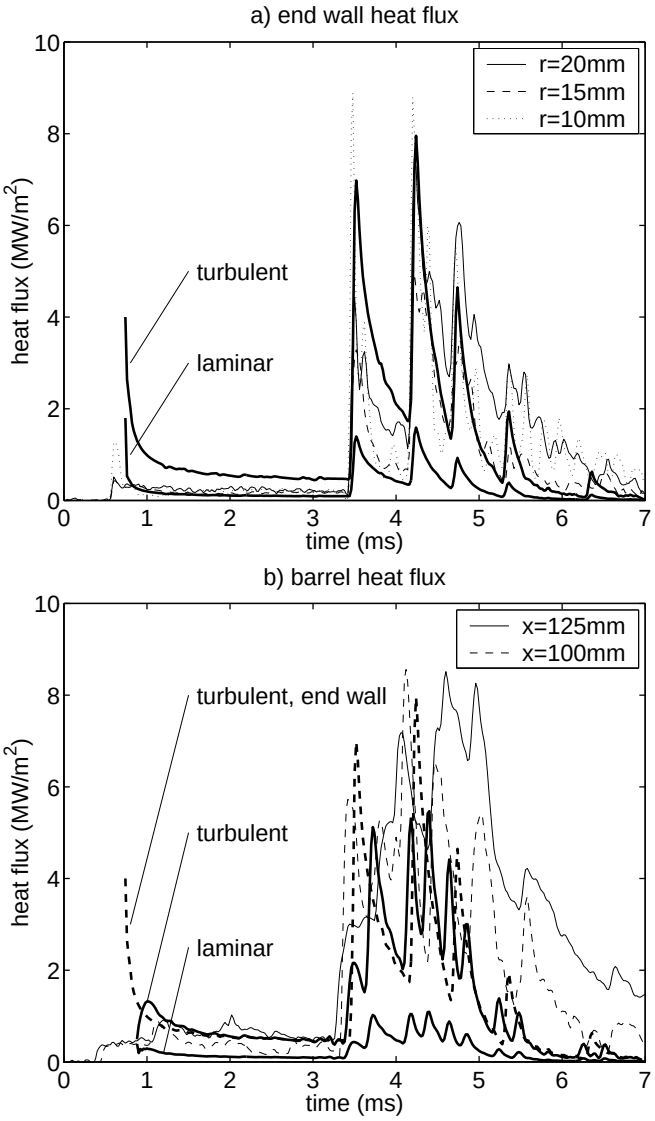

Figure 3: Heat flux at the end wall (part a) and in the barrel (part b).

[Groth et al., 1991] Groth CPT, Gottlieb JJ, Sullivan PA (1991) Numerical investigation of high-temperature effects in the UTIAS-RPI hypersonic impulse tunnel. Canadian Journal of Physics 69:897–918

[Isshiki and Nishiwaki, 1970] Isshiki N, Nishiwaki, N (1970) Study on laminar heat transfer of inside gas with cyclic pressure change on an inner wall of a cylinder head. Heat Transfer 1970: Proc. 4th Int. Heat Transfer Conf., Paris and Versailles, FC3.5, pp.1–10, U. Grigull and E. Hahne (Eds), Elsevier, Amsterdam

[Jacobs, 1994] Jacobs PA (1994) Quasi-one-dimensional modeling of a free-piston shock tunnel. AIAA Journal 32:137–145

[Kendall et al., 1997] Kendall MA, Morgan RG, Jacobs, PA (1997) A compact shock-assisted free-piston driver for impulse facilities. Shock Waves 7:219–230

[Knöös, 1971] Knöös S (1971) Theoretical and experimental study of piston gas-heating with laminar energy losses. AIAA Journal 9:2119–2127

[Lawton (1987)] Lawton B (1987) Effect of compression and expansion on instantaneous heat transfer in reciprocating internal combustion engines. Proc IMechE Part A Power and Process Engineering 201:175–186

[Oldfield et al., 1982] Oldfield MLG, Burd HJ, Doe NG (1982) Design of Wide-Bandwidth Analogue Circuits for Heat Transfer Instrumentation in Transient Wind Tunnels. Proceedings 16th Symp. of International Centre for Heat and Mass Transfer, Hemisphere Publishing, pp. 233-257

[Oude Nijeweme et al., 2001] Oude Nijeweme DJ, Kok JBW, Stone CR, Wyszynski L (2001) Unsteady in-cylinder heat transfer in a spark ignition engine: experiments and modelling. Proc IMechE Part D Journal of Automobile Engineering 215:747-760

[Tani et al., 1994] Tani K, Itoh M, Takahashi M, Tanno T, Komuro T, Miyajima H (1994) Numerical study of free-piston shock tunnel performance. Shock Waves 3:313–319